J Fluoresc (2016) 26:283–295
DOI 10.1007/s10895-015-1712-0

ORIGINAL ARTICLE

Interaction of Graphene Quantum Dots with 4-Acetamido-2,2,6,6-Tetramethylpiperidine-Oxyl Free Radicals: A Spectroscopic and Fluorimetric Study

Ojodomo J. Achadu[1] · **Tebello Nyokong**[1]

Received: 10 August 2015 / Accepted: 26 October 2015 / Published online: 9 November 2015

Abstract We report on the interaction of graphene quantum dots (GQDs) with 4-acetamido-2,2,6,6-tetramethylpiperidine-oxyl (4-acetamido-TEMPO) free radicals. The GQDs were N and S, N doped. The fluorescence quantum yields were higher for the doped GQDs compared to the undoped. The interaction is assessed by spectrofluorimetric, steady state/time resolved fluorescence and electron paramagnetic resonance (EPR) techniques. Fluorescence quenching was observed upon the addition of 4-acetamido-TEMPO to the GQDs. Photo-induced electron transfer (PET) mechanism was suggested as the plausible mechanism involved in the fluorescence quenching in which 4-acetamido-TEMPO acted as the electron acceptor.

Keywords Graphene quantum dots · Free radicals · Fluorescence quenching · Stern-volmer quenching constant

Introduction

Graphene quantum dots (GQDs) are luminescent carbon based nanomaterials [1]. Typically, GQDs have diameters within the range of 3–20 nm. The presence of quantum confinement and edge effects make GQDs possess properties such as tunable band gap and high photoluminescence activity [2]. GQDs exhibit superior characteristics compared to the conventional semiconductor quantum dots such as excellent biocompatibility, low toxicity, good water dispersibility [3], chemical stability, large optical absorptivity, high fluorescence activity and excellent photostability [4].

GQDs are rising carbon based photoluminescent nanomaterial that have garnered applications in areas such as bioimaging, chemical sensing, catalysis, biosensors, photovoltaics and photodynamic therapy (PDT) [3, 5]. Photoluminescence (PL) properties of GQDs may be tuned through surface passivation, functionalization, doping with hetero atoms (B, N, S or SN) or capping etc. [6–8].

Quenching of GQDs fluorescence by different classes of compounds such as proteins [9–11], metal ions [12] and organic compounds [13, 14] has been reported. The tendency to suppress or quench the fluorescence intensity of GQDs upon interaction with these compounds has led to the fabrication of GQDs based nanosensors. Studies on the use of GQDs to scavenge reactive oxygen species (ROS) are sparse or non-existent. Conventional semiconductor quantum dots (which contain heavy metals) have often been used as free radicals scavengers [15, 16], but their application in vivo is impeded due to their high cytotoxicity. GQDs do not have the toxicity of conventional QDs.

To demonstrate the proof-of-concept of sensing properties of GQDs, the interaction of GQDs with N-oxide free radicals is presented in this work. To the best of our knowledge, this is the first time interactions of GQDs, N-doped GQDs (N-GQDs) and SN-doped GQDs (SN-GQDs) with 4-acetamido-2,2,6,6-tetramethylpiperidine-oxyl (4-acetamido-TEMPO) free radicals are reported. We report that the fluorescence of GQDs and the N and SN doped nanohybrids can be efficiently quenched by 4-acetamido-TEMPO.

Electronic supplementary material The online version of this article (doi:10.1007/s10895-015-1712-0) contains supplementary material, which is available to authorized users.

✉ Tebello Nyokong
t.nyokong@ru.ac.za

[1] Department of Chemistry, Rhodes University, Grahamstown 6140, South Africa

Experimental

Materials

Citric acid, sodium hydroxide pellets, and urea were obtained from Merck. 4-Acetamido-2,2,6,6-tetramethylpiperidine-oxyl (4-acetamido-TEMPO), Rhodamine 6G and dialysis tubing (MWCO 1.5 kDa) were obtained from Sigma Aldrich. Thiourea was obtained from Fluka. All chemicals were of analytical grade and used without prior purification. All solutions were prepared with ultra-pure water obtained from a Mili-Q Water system (Milipore Corp. Bedford, MA, USA). All other reagents were obtained from commercial suppliers and used as received.

Instrumentation

Excitation and emission spectra were recorded on a Varian Eclipse spectrofluorimeter. The excitation wavelengths and slit width (each 5 nm) were kept constant for all the experiments. Ground state electronic absorption spectra were performed on a Shimadzu UV-2550 spectrophotometer in the range 200–800 nm. Infra-red spectra were collected on a Perkin Elmer Spectrum 100 FT-IR Spectrometer. A Metrohm Swiss 827 pH meter was used for pH measurements.

X-ray photoelectron spectroscopy (XPS) analysis was done using an AXIS Ultra DLD (supplied by Kratos Analytical) using Al (monochromatic) anode equipped with a charge neutralizer, the following parameters were used: the emission was 10 mA, the anode (HT) was 15 kV and the operating pressure below 5×10^{-9} Torr. A hybrid lens was used and resolution to acquire scans was at 160 eV pass energy in slot mode. The center used for the scans was at 520 eV (width of 1205 eV) with steps at 1 eV and dwell time at 100 ms. The high resolution scans were acquired using 80 eV pass energy in slot mode. The chemically distinct species were resolved using a nonlinear least squares curve fitting procedure. The core level binding energies (BEs) were aligned with respect to the C 1 s binding energy (BE) of 284.5 eV.

X-ray powder diffraction patterns were recorded on a Bruker D8 Discover equipped with a Lynx Eye detector, using Cu-K_α radiation (l = 1.5405 A°, nickel filter). Data were collected in the range from $2\theta = 10^{\circ}$ to 50°, scanning at 1° min^{-1} with a filter time-constant of 2.5 s per step and a slit width of 6.0 mm. Details have been provided before [17]. Fluorescence lifetimes were measured using a time correlated single photon counting setup (TCSPC) (FluoTime 200, Picoquant GmbH) with a diode laser (LDH-P-485 with 10 MHz repetition rate, 88 ps pulse width) as described before [17].

A Bruker Vertex 70-Ram II Raman spectrometer (equipped with a 1064 nm Nd:YAG laser and liquid nitrogen cooled germanium detector) was used to collect Raman data. Thermo-gravimetric analysis (TGA) was performed using a Perkin Elmer TGA 4000 analyzer. The analysis was carried out under nitrogen flow rate of 120 $cm^{-3}min^{-1}$. The weighed sample masses were heated from 50 to 850 °C at a heating rate of 10 °C min^{-1}. Transmission electron microscope (TEM) micrographs for the quantum dots were obtained using a Zeiss Libra 120 TEM operating at 80 kV.

Energy dispersive spectroscopy (EDS) was carried out using an INCA PENTA FET coupled to VAGA TESCAN using a 20 kV accelerating voltage.

Hydrothermal synthesis was carried out using a Berghof (Germany) High Pressure Laboratory Reactor BR-300, V.3.0 equipped with PT-100 temperature and pressure sensors, BTC-300 Temperature regulator and manometer and PTFE lining.

Electron paramagnetic resonance (EPR) measurements were carried out using a Bruker EMX Plus EPR spectrometer, model number: EMP-9.5/12B/P. EPR settings were 0.632 mW for the microwave power, frequency 9.714 GHz, resolution 2048 points, centre field 3460 G and 100 G for the sweep width.

Synthesis of Graphene (GQDs), N Doped Graphene (N-GQDs) and SN co-Doped Graphene (SN-GQDs) quantum Dots

GQDs, N-GQDs and SN-GQDs were synthesized by hydrothermal method adopted from the literature with some modifications [18, 19]. Briefly;

GQDs: 4.2 g (1 mmol) citric acid and 2.4 g (3 mmol) NaOH were dissolved in 100 mL water, and stirred to form a clear solution. Then the solution was transferred into a 400 mL Teflon lined stainless autoclave. The sealed autoclave was heated to 160 °C for 4 h. The final product was collected by adding ethanol into the solution and centrifuged at 5000 rpm for 15 min. The solid was re-dispersed into water and was dialyzed for two days using a dialysis membrane (MW 1.5 kDa) to remove excess salts.

N-GQDs: were prepared as described above for pristine GQDs, using 3.6 g (3 mmol) urea in place of NaOH.

SN-GQDs: these were also prepared as described above for pristine GQDs, using 4.6 g (3 mmol) thiourea instead of NaOH.

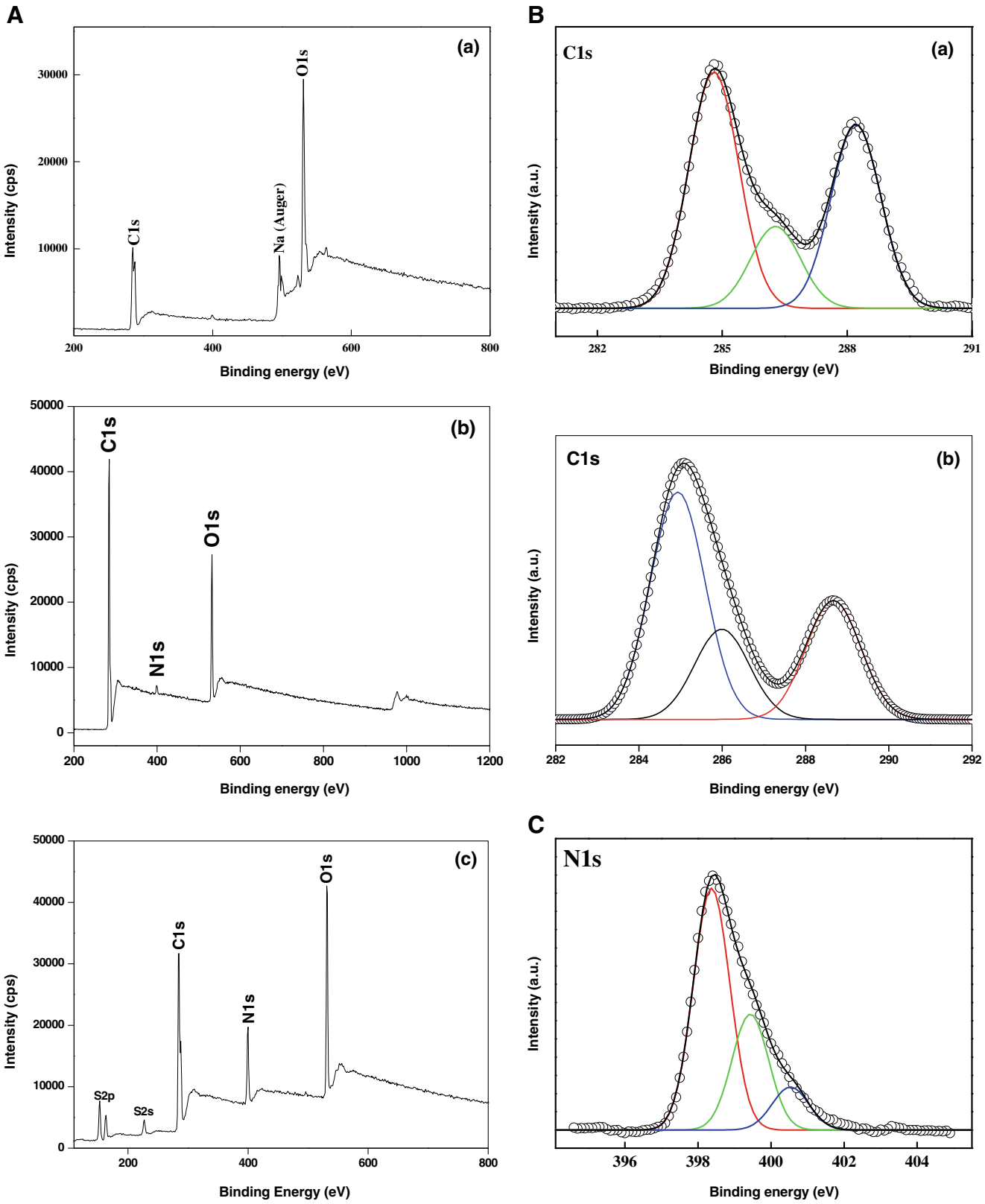

Fig. 1 **A** XPS full survey spectrum of (*a*) GQDs, (*b*) N-GQDs and (*c*) SN-GQDs; **B** High resolution spectrum of C1s of (*a*) GQD and (*b*) SN-GQDs, and **C** High resolution spectrum of N1s of SN-GQDs

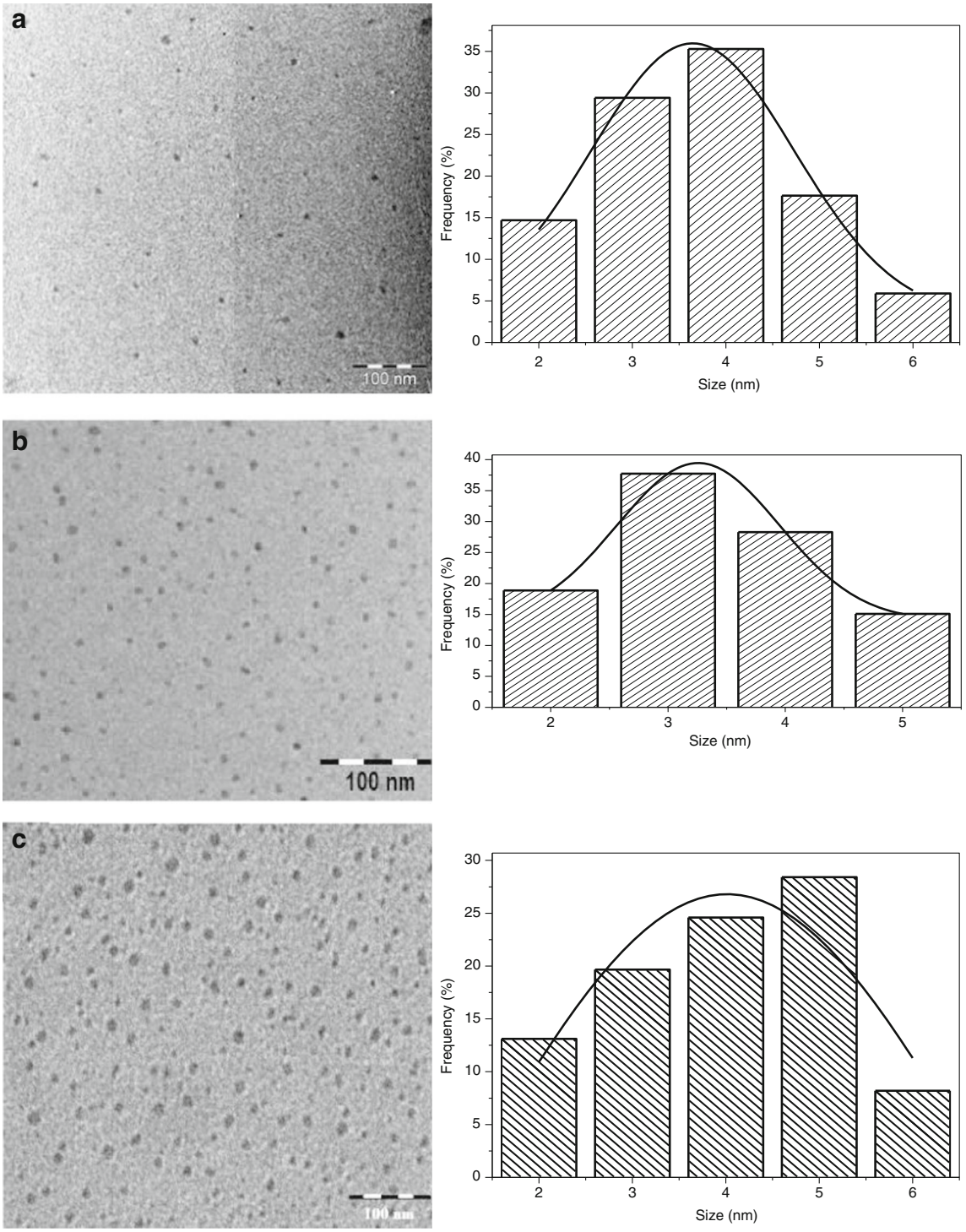

Fig. 2 TEM images of **a** pristine GQDs, **b** N-GQDs and **c** SN-GQDS with the corresponding histograms

Fluorescence Studies

Fluorescence Quantum Yields

Fluorescence quantum yields of the GQDs were determined by the comparative method [20], Eq. 1.

$$\Phi_{\mathrm{F}} = \Phi_{\mathrm{F}}^{Std} \frac{\mathrm{F.A}^{Std}.\mathrm{n}^2}{\mathrm{F}^{Std}.\ \mathrm{A}.(\mathrm{n}^{Std})^2} \quad (1)$$

Where A and A^{Std} are the absorbances of the sample and the standard at the excitation wavelength, respectively. F and F^{Std} are the areas under the fluorescence curves of the GQDs and

the standard, respectively and n and n^{Std} are the refractive indices of the solvent used for the sample and standard, respectively. Rhodamine 6G in ethanol ($\Phi_F^{Std} = 0.94$ [21]) was used as the standard.

Fluorescence Quenching Experiments

Colloidal aqueous solutions (2 mL, 1 mg/mL) of GQDs, N-GQDs and SN-GQDs were mixed with various concentrations of 4-acetamido-TEMPO (2.0–20.0 μM) in 50 mM phosphate buffer solution (PBS) (pH 9.2). This pH was employed since GQDs are not fluorescent in acid media [22]. The fluorescence spectra of the GQDs, N-GQDs and SN-GQDs were recorded under excitation wavelengths of 350, 360 and 390 nm for GQDs, N-GQDs and SN-GQDs, respectively. The working solutions were vigorously stirred prior to photoluminescence measurements at room temperature. For temperature dependent fluorescence quenching studies, temperature was varied from 25 °C to 40 °C. The real temperature of the solution inside the quartz cell was measured using a probe thermocouple.

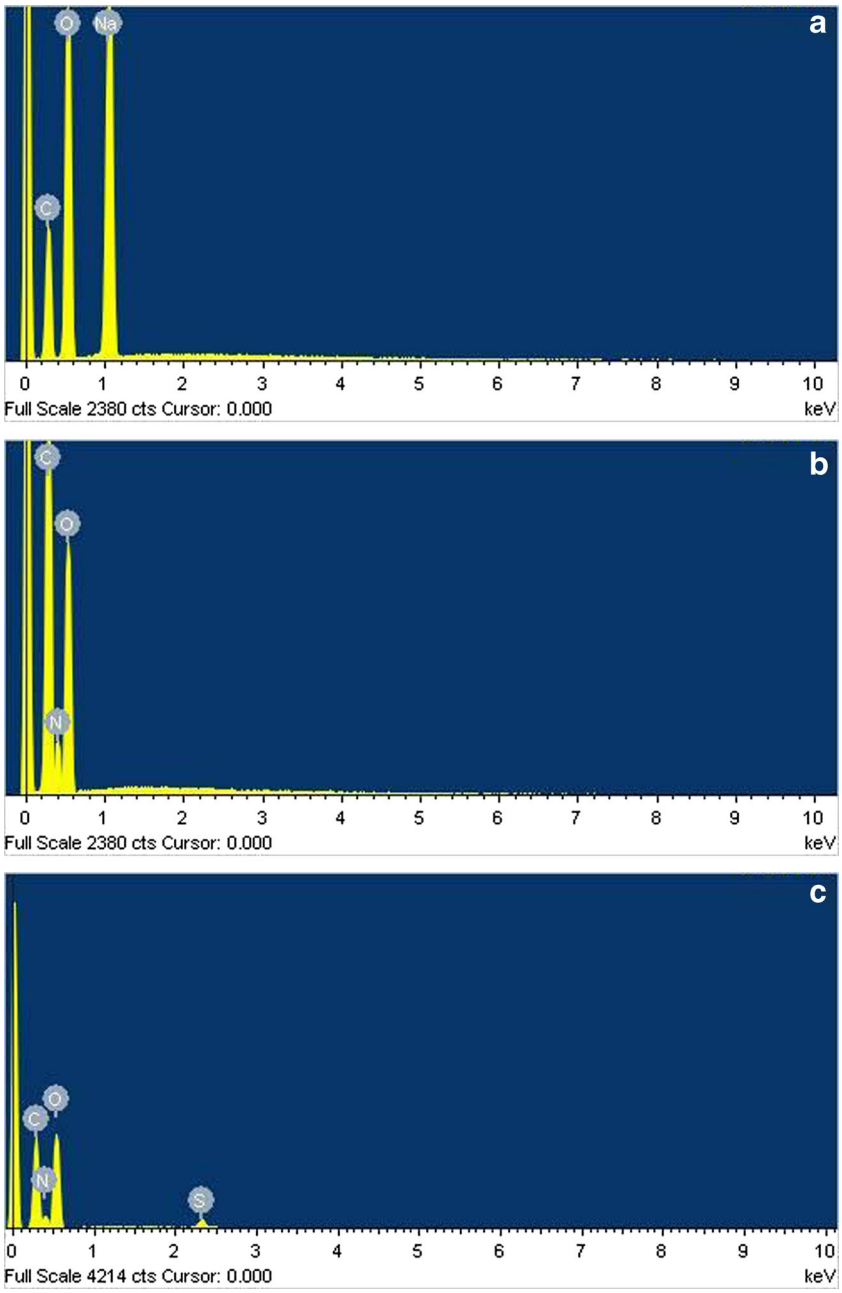

Fig. 3 EDS of **a** pristine GQDs, **b** N-GQDs and **c** SN-GQDS

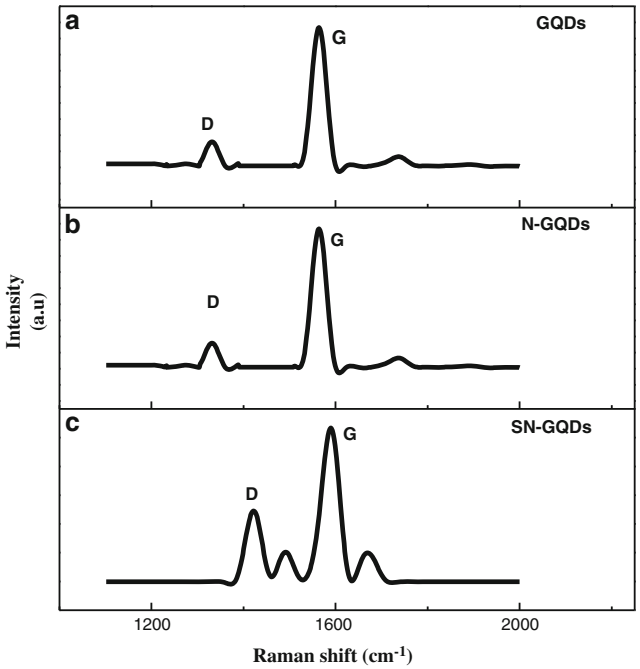

Fig. 4 Raman spectra of GQDs **a** pristine GQDs, **b** N-GQDs and **c** SN-GQDS

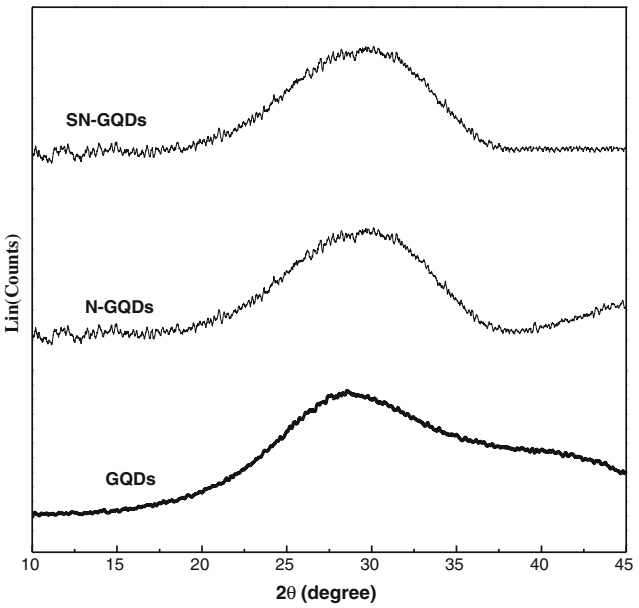

Fig. 6 XRD of SN-GQDS, N-GQDs and GQDs

Results and Discussion

Characterization of as Synthesized GQDs, N-GQDs and SN-GQDs

X-ray Photoelectron Spectroscopy (XPS)

X-ray photoelectron spectroscopy (XPS) analysis was carried out to probe the structural compositions of the GQDs, N-GQDs and SN-GQDs. Full scan XPS spectrum of GQDs shows C1s, Na auger and O1s signals at 284.5, 496 and 530 eV, respectively (Fig. 1**A**(*a*)). Na auger peak at 496 eV is as a result of NaOH employed in the GQDs synthesis. The full survey XPS spectra of N-GQDs and SN-GQDs (Fig.1**A**(*b*) and (*c*)), show peaks at 530, 398 and 284.5 eV corresponding to O1s, N1s and C1s in both N-GQDs and SN-GQDs respectively. However, the wide scan survey of SN-GQDs showed extra peaks at 227 and 162 eV attributed to S2s and S2p signals, respectively (Fig. 1**A**(*c*)). The appearance of N1s (for N-GQDs) and N1s, S2s and S2p (for SN-GQDs) in the full survey spectra, relative to that of the pristine GQDs confirm the successful doping of the GQDs.

The core level high-resolution C1s XPS spectrum of GQDs could be deconvoluted into three chemically distinct carbon species centered at 284.5, 286.2, and 288.4 eV, which was attributed to sp^2 C (C-C, C = C), sp^3 C (C-O) and oxidized C (C = O), respectively and shown in Fig. 1**A**(*a*). The C1s signal of the SN-GQDs was deconvoluted (Fig.1**B**(*b*)) which shows three distinct carbon species belonging to sp^2 hybridized carbons (C = C) in graphene at 284.9 eV, sp^3 carbons (C-S, C-N and C-O) were found at 286.2 eV and oxidized carbons (C = O)

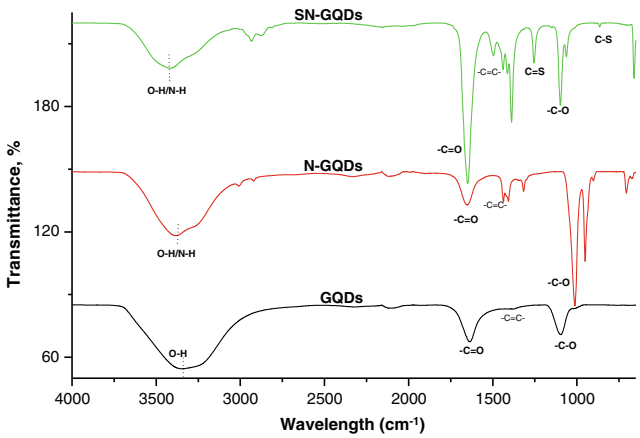

Fig. 5 FT-IR spectra of the synthesized GQDs, N-GQDs and SN-GQDs

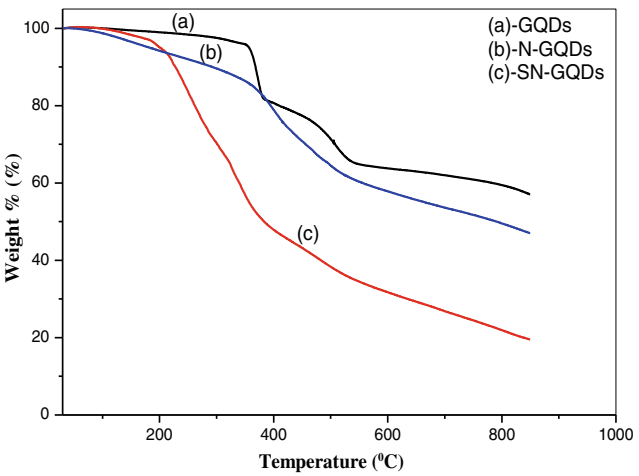

Fig. 7 TGA profiles of the GQDs and its doped analogues

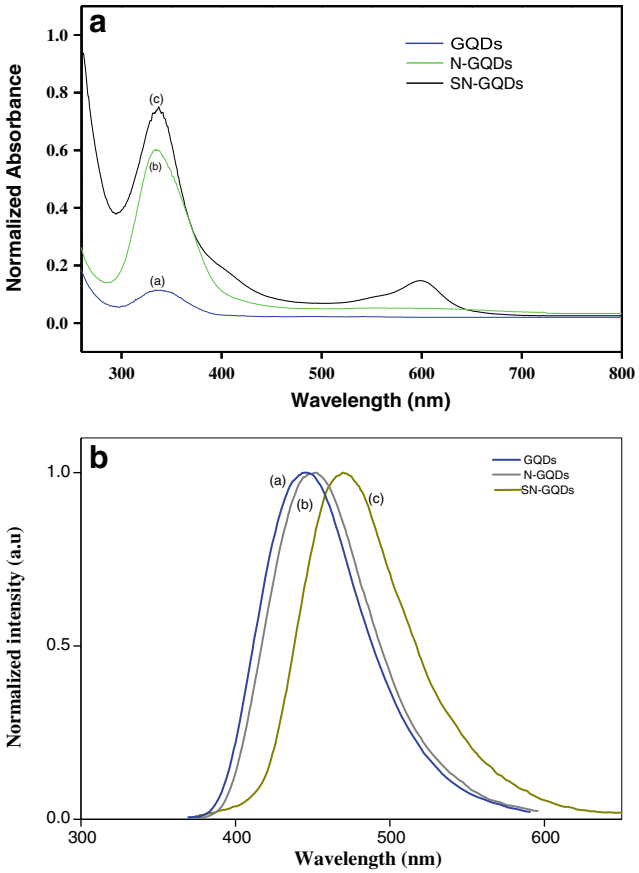

Fig. 8 Overlay of **a** UV-Vis and **b** PL spectra of pristine GQDs, excitation at 350 nm (*a*) N-GQDs, excitation at 360 nm (*b*) and SN-GQDs, excitation at 390 nm (*c*). pH 9.2 buffer

were found at 288.6 eV. Deconvoluted C1s XPS spectrum for N-GQDs is shown in Fig. S1a (Supporting information).

High resolution of N1s for SN-GQDs displayed peaks attributed to C-N-C-) at 398.5 eV and graphitic N at 399.7 and N-H peak at 400.5 eV, respectively (Fig. 1C). The deconvoluted S2p peak (which was not observed in GQDs and N-GQDs) from the full survey scan further shows three distinct peaks at 162.4, 163.8 and 165.1 eV, respectively (Fig. S1(b) Supporting information). These implies the incorporation of S into the GQDs structure and indicates that the GQDs are doped with S. XPS results obtained for GQDs, N-GQDs and SN-GQDS in this study conform closely with what has been reported in the literature [18, 19].

TEM and EDS Analysis

Transmission electron microscopy (TEM) images (Fig. 2) show the monodispersed nanoparticles of the as-synthesized GQDs in the range 2–6 nm size distribution. These size distributions for GQDs and its doped analogues have been reported [3, 18, 23, 24].

Energy Dispersive Spectroscopy (EDS) was used to check the elemental composition of the as prepared GQDs (Fig. 3). Results obtained were consistent with the expected elemental compositions of the pristine GQDs, N-GQDs and SN-GQDs respectively, which further confirm the successful doping of the GQDs. For pristine GQDs, the C and O are from the core quantum dots. The Na is from the NaOH (as a base) employed in the synthesis. For N-GQDs, the C and O are from the core QDs, and the N is from N doping using urea. For SN-GQDs, the C, N and O are as explained for N-GQDs. The S is from S doping using thiourea.

Raman Spectra

The Raman spectra of the as-prepared GQDs were also acquired, which revealed characteristic D and G bands (Fig. 4). This further gives insight as to the quality of the GQDs. N-GQDs show the disordered (D) band at 1365 cm^{-1}, related to the presence of sp^3 defects, and the crystalline (G) band at 1573 cm^{-1} related to the in-plane vibration of sp^2 carbon. In the case of the SN-GQDs, the D and G bands were found at 1420 and 1579 cm^{-1}, respectively. These shifts might due to the cooperative defect (SN-doping) introduced into the lattices and stretching of the graphene layers by doping which has been previously observed [25]. The ratio of the intensities (I_D/I_G) of D and G bands has been used to correlate the structural properties of the carbon based nanomaterials [19]. The I_D/I_G ratios for N-GQDs and SN-GQDs were found to be 0.62 and 0.77 respectively, as compared to 0.51 obtained for the pristine GQDs. These values are close to previously reported values for GQDs (N and SN-GQDs) [19]. Thus, the disorder sp^3 increases with doping. The extra peaks in Fig. 4c could be due to luminescence background [25].

Table 1 Fluorescence quantum yield (Φ_F), Stern-Volmer quenching constant (K_{SV}), bimolecular quenching constant (k_q), excitation and emission wavelengths maxima for GQDs, N-GQDs and SN-GQDs

Sample	$\lambda_{absorption}$ (nm)	$\lambda_{emission}$ (nm)	Φ_F	K_{SV} (M^{-1})	PL Lifetimes (ns)	k_q ($dm^3\ mol^{-1}\ s^{-1}$)
GQDs	335	445	0.21	1.27×10^4	5.7	2.49×10^{13}
N-GQDs	340	450	0.77	1.5×10^5	7.8	2.03×10^{13}
SN-GQDs	337,550,598	470	0.81	1.7×10^5	11.6	1.52×10^{13}

FT-IR

FT-IR spectra of the GQDs reveal the presence of functional groups usually at the edges of graphene quantum dots. FT-IR analysis was used to characterize and ascertain the surface functional groups present on the GQDs, N-GQDs and SN-GQDs. The FT-IR spectra (Fig. 5) show broad absorption bands in all the synthesized GQDs from 3000 to 3500 cm^{-1} which are characteristic absorption bands for O–H stretching vibrations. Thus, it can be inferred that hydroxyl groups are present on the surface of the pristine GQDs. It is possible that both N–H and/or O–H groups are present in the spectra of the doped GQDs (N-GQDs and SN-GQDs). It is also noteworthy that the presence of these hydrophilic functional moieties confers on the GQDs their excellent water dispersibility.

The bands at 1625 cm^{-1} are attributed to the vibrational band of C = O in COOH for all the GQDs. The peak around 1203 cm^{-1} in SN-GQDs is attributed to the C = S. Weak C–S stretching was observed at 635 cm^{-1}.

X-ray Diffraction (XRD) Analysis

X-ray diffraction analysis was further used to verify the structural configuration of the synthesized GQDs. GQDs generally show a broad peak of (002) plane of hexagonal graphite [26, 27]. XRD profiles of GQDs, N-GQDs and SN-GQDs exhibit similar peaks around 25^0 (Fig. 6) thus confirming similar graphitic structural base and is consistent with previous structural analysis on GQDs [26, 27]. However, the XRD patterns of the doped GQDS (N-GQDs and SN-GQDs) show broader peaks indicating the presence of surface defects on the graphitic structure or depleted oxygen groups as a result of the doping.

TGA Analysis

Thermal properties of the as synthesized GQDs were investigated. The data obtained showed that the GQDs displayed high degree of stability. Generally, from the TGA curves (Fig. 7) pristine GQDs showed the most stability with increasing temperature. N-GQDs was found to be more stable than the SN-GQDs. This can be ascribed to the N and SN dopants elimination processes taking place as the temperature increases. Weight loss processes at higher temperatures (c.a 400–850 °C) could be due to the relaxation of the graphene structure.

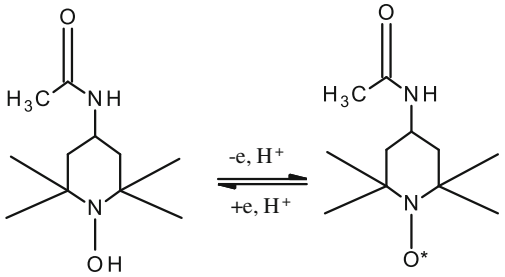

Scheme 1 Structural transformation of nitroxide radicals into diamagnetic hydroxylamine and oxoammonium cation upon electron transfer

Optical Properties of GQDs, N-GQDs and SN-GQDs

The effect of pH on the PL properties of GQDs is well documented in the literature [5, 8, 22, 26]. Strong emissions are observed in alkaline media, whereas in acidic conditions PL of GQDs is almost completely quenched [26], due to reduced stability [22] in the latter, hence basic media is employed in this work.

The UV-Vis spectral peaks were observed at 335 nm (for pristine GQDs), 340 nm for N-GQDs and 337, 550 and 598 nm (for SN-GQDs), all dispersed in aqueous medium (Fig. 8a, Table 1). The red shifting of the peak near 340 nm for N-GQDs and SN-GQDs when compared to pristine GQDs can be ascribed to changes in chemical functionalities and defects as reported before [28]. The appearance of absorption peaks at 550 and 598 nm in SN-GQDs absorption spectrum is due to the doping with sulfur (Fig. 8a(*c*)) which has been reported before [19].

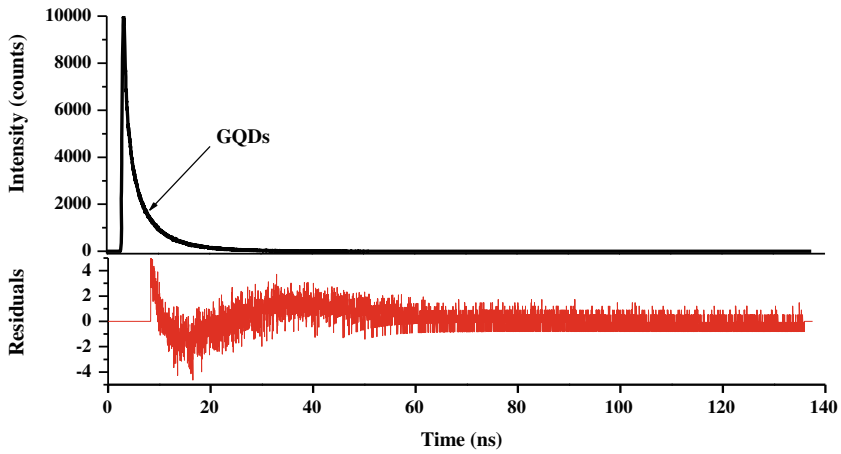

Fig. 9 Fluorescence decay curve for pristine GQDs

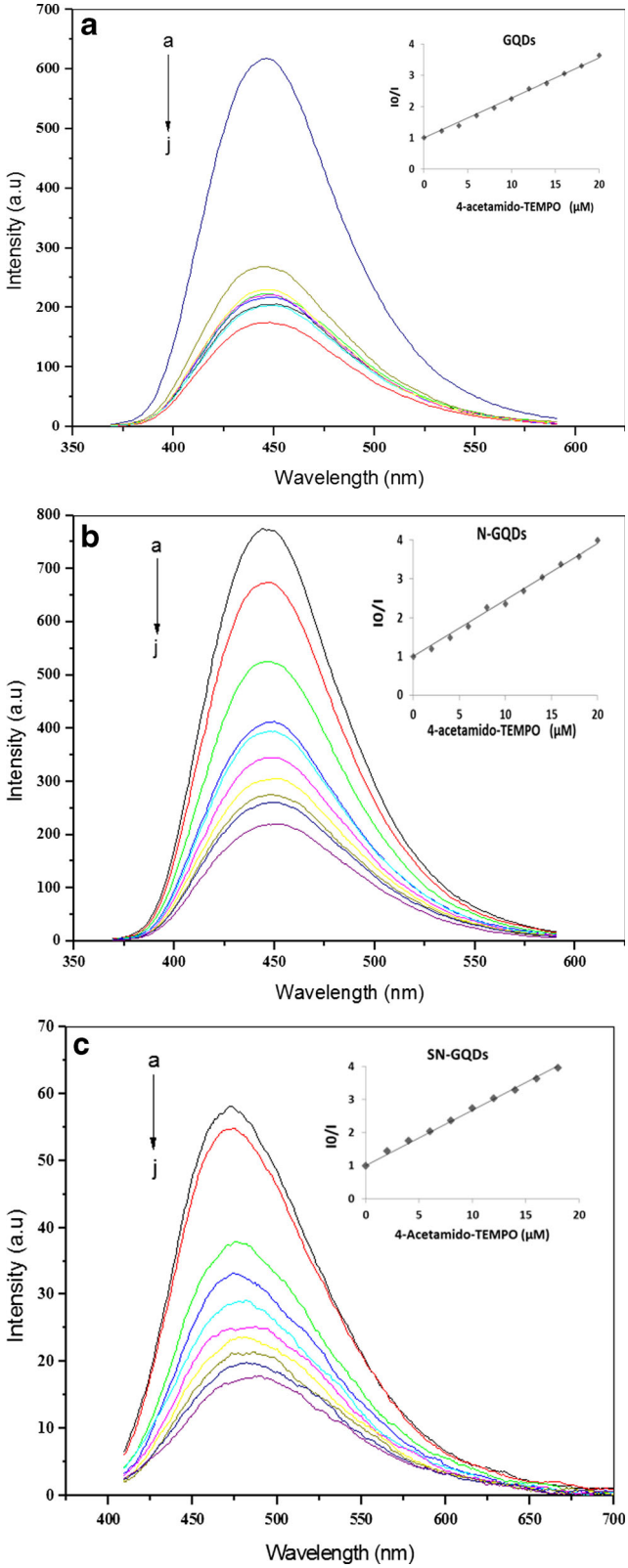

◀ **Fig. 10** **a** Emission spectra of pristine GQDs, **b** N-doped GQDs and **c** SN-doped GQDs in the presence of various concentrations of 4-acetamido-TEMPO in PBS buffer (pH 9.2) solution. [4-acetamido-TEMPO] a-j: 2.0, 4.0, 6.0, 8.0, 10.0, 12.0, 14.0, 16.0, 18.0, 20.0 μM. Corresponding Stern-Volmer plots shown as inserts. Starting concentration of GQDs =2 mL of 1.0 mg/mL

GQDs may exhibit excitation wavelength dependent (where there is a change in emission wavelength with changes in excitation wavelength) or independent (where there is no change in emission wavelength, but there may be a change in intensity) PL [9, 19, 26, 29]. The excitation-dependent emission PL is proposed to reflect the differences in nanoparticle sizes and also the presence of a mixture of different emissive sites [19]. Conversely, excitation wavelength independent emissions in GQDs have been ascribed to the uniformity in both size and surface states. In this work, the pristine GQDs were excited at wavelengths from 300 to 380 nm with emission wavelength peaking at 445 nm, Fig. 8 b(a), Table 1. Since emission wavelength did not change with change in excitation wavelength, the GQDs are excitation wavelength independent, suggesting a uniform size. Maximum emission intensity was recorded at an excitation wavelength of 350 nm. Further studies were carried out at this wavelength of maximum PL intensity.

N-GQDs and SN-GQDs both exhibit excitation independent PL behavior. Similar to pristine GQDs, their PL intensities were however affected by different excitation wavelengths. These further affirm that both N-GQDs and SN-GQDs should be of uniform size and have similar PL originating from the core of graphene layers. N-GQDs showed maximum emission at 450 nm at an excitation wavelength of 360 nm, Fig. 8b(*b*). When compared to the PL emission maximum of pristine GQDs, a red shift of ca 5 nm is observed, corresponding to the red shift in the electronic absorption spectra. In addition, PL shifts in GQDs may be due to lowering of band gaps as a result of increased electron density to the sp^2 clusters of graphene layers [8, 30]. SN-GQDs recorded a maximum emission at 470 nm (Fig. 8b(c) Table 1) at an excitation wavelength of 390 nm. When compared to the PL emission maximum of the GQDs, a red shift of ca 25 nm is observed which can be attributed to an increase in the electron density introduced via the hetero atomic SN-doping, due to increased electron density to the sp^2 clusters of graphene layers, as a result of the presence of both N and S atoms [29].

The co-doped GQDs (SN-GQDs) has the highest Φ_F value of 0.81 (Table 1). This value is close to reported Φ_F value in previous reports [19]. PL of GQDs can be attributed to the radiative recombination of electrons and holes trapped on the surface of GQDs [30, 31]. Comparing the fluorescence quantum yields of the doped-GQDs to pristine GQDs, it can be observed that the doped analogues have Φ_F values which are much higher. This further relates to the fact that N-GQDs and SN-GQDs should have the same PL origin, which is different from the pristine GQDs.

Fluorescence lifetimes were found to be single exponential decay (Fig. 9, Table 1). The fluorescence lifetimes for doped N-GQDs and SN-GQDs are longer than for pristine GQDs corresponding to larger fluorescence quantum yields. Even though the origin of PL in GQDs is not yet completely understood, it has been clearly argued that the presence of oxygen rich groups (hydroxyl, carbonyls and carboxyls) on the layers or intercalated within the lattice structure of the graphene, provide GQDs with surface states and emissive traps for PL properties. On the other hand, enhancement in PL properties such as quantum yields, PL emissions and exponential lifetime decay resulting from doping or surface functionalization has been attributed to the introduction of new kinds of surface states [27]. Specifically, N-doping of GQDs where N atoms are intercalated into the graphitic core and/or anchored on the edges, results in the introduction of a new surface state (denoted as the N-state). These new states have emissive traps that are able to promote a high yield of radiative recombination [32].

Quenching of GQDs Fluorescence by 4-Acetamido-TEMPO

4-Acetamido-TEMPO gets reduced in acidic media forming stable hydroxylamine derivative [33] (Scheme 1). There is no protonation in alkaline media. Hence, we carried out our studies in alkaline pH of 9.2 PBS buffer solutions which is also the pH used for GQDs.

GQDs may interact with other molecules through π-π stacking, electrostatic interaction, and chemical bonding [34], resulting in quenching of the GQDs fluorescence. Stable free radicals are known fluorescence quenchers and are used in this work to quench GQDs fluorescence. For quenching experiments, aqueous buffered solutions of GQDs, N-GQDs and SN-GQDs were mixed with varying concentrations of 4-acetamido-TEMPO.

Figure 10 shows the quenching of the GQDs, N-GQDs and SN-GQDs PL emissions upon addition of various amounts of 4-acetamido-TEMPO. The PL intensity gradually decreased as the concentration of the 4-acetamido-TEMPO was increasingly varied. Changes were not observed in the spectral peak width or emission wavelength maxima of the fluorescence spectra recorded for all the GQDs. Charge/energy transfer leading to non-radiative relaxation due to the collision of the excited electrons with quencher molecules has been proposed to lead to quenching of the fluorescence in GQDs [35, 36]. It is expected that 4-acetamido-TEMPO and GQDs are in close proximity, resulting in photoinduced electron transfer (PET) from the latter to the former, Scheme 2.

The quenching of the fluorescence of GQDs and its doped counterparts by 4-acetamido-TEMPO free radical can be described by the Stern-Volmer equation (Eq. 2):

$$\frac{I_0}{I} = 1 + K_{SV}[Q] \tag{2}$$

where I_0 and I are the PL intensities of GQDs in the absence and presence of 4-acetamido-TEMPO, respectively. K_{sv} is the Stern–Volmer quenching rate constant which is related to the quenching efficiency. The K_{sv} values were obtained from the slopes of the Stern-Volmer plots (inserts in Fig. 10) and are listed in Table 1. The K_{sv} value of SN-GQDs is the highest in Table 1, suggesting that the fluorescence of SN-GQDs is most efficiently quenched by the free radical interaction. This might be attributed to the following possible reasons: (a) the disruption of the electrical neutrality of the sp^2-hybridized carbon atoms of the SN-GQDs graphene core by the electron rich N and S atoms, leads to charged sites within the intrinsic states which favor more interaction with the free radicals. (b) The S and N atoms on SN-GQDs introduce new surface states thus creating emissive traps from electron-hole recombination, the interaction of the new surface states with the free radicals could prevent the exciton electron from recombining due to the transfer of the electron to the free radical molecules.

The bimolecular quenching constant k_q may be determined using Eq. 3

$$K_{SV} = k_q \tau_F \tag{3}$$

where τ_F is the fluorescence lifetime of 4-acetamido-TEMPO. The k_q values are higher (being in the order of 10^{13} dm^3 mol^{-1} s^{-1}, Table 1) than the proposed value for dynamic quenching (10^{10} dm^3 mol^{-1} s^{-1}) [37] indicating that the quenching mechanism in this case is static. The Stern-Volmer quenching constants (K_{SV}) (Table 2) were inversely related to temperature, which indicates that the probable

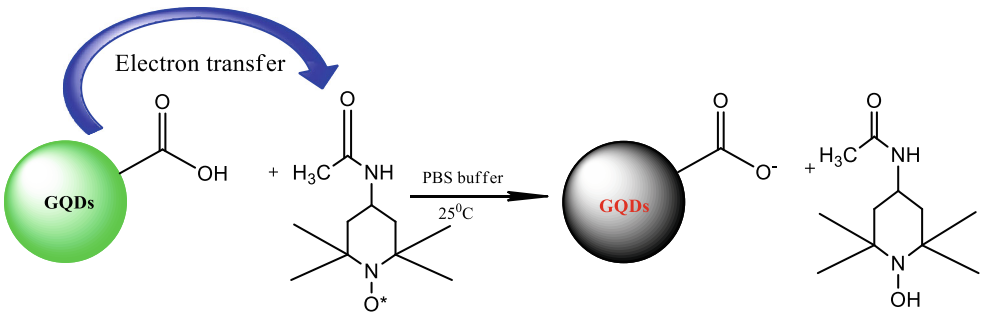

Scheme 2 Plausible Interaction mechanism between GQDs and 4-acetamido-TEMPO

quenching mechanism to be initiated by complex formation rather than by dynamic collision [38].

Decay Kinetics of 4-Acetamido-TEMPO in the Presence of GQDs

To further understand the nature of the interaction of the GQDs with 4-acetamido-TEMPO, we recorded changes in the UV-Vis absorption spectra of 4-acetamido-TEMPO with time in the presence of GQDs, N-GQDs and SN-GQDs (Fig. 11). The absorption peak at 426 nm for 4-acetamido-TEMPO, gradually decrease with time following addition of fixed concentrations of GQDs (Fig. 11). A new peak was formed near 340 nm. The spectral changes in Fig. 11 confirm the formation of a ground state complex between GQDs and 4-acetamido-TEMPO. The new product which absorbs near 340 nm was not fluorescent. It is most likely hydroxylamine (Scheme 1).

EPR Studies

EPR analysis was carried out to further elucidate the interactions between 4-acetamido TEMPO free radicals and GQDs (N-GQDs and SN-GQDs) as shown in Fig. 12. As confirmed above, a ground state complex is formed between 4-acetamido TEMPO and the GQDs. There was no clear EPR signal of the 4-acetamido-TEMPO upon interaction with the GQDs (Fig. 12). The results confirm that the product is not a radical; we suggest that it is hydroxylamine as stated above.

Conclusions

We report the facile synthesis of graphene quantum dots and its doped nano-hybrids by the bottom-up hydrothermal synthesis. The interactions of nitroxide free radicals (4-acetamido-TEMPO) with the highly fluorescent GQDs and its N and SN-doped nanohybrids in aqueous buffer solution were studied by spectroscopic, fluorimetric, kinetic, steady state/time resolved measurements and EPR techniques. The fluorescence of the GQDs were found to be efficiently quenched by 4-acetamido-TEMPO. Photo-induced electron transfer mechanism was suggested as the plausible mechanism involved in the fluorescence quenching in which 4-

Table 2 Quenching constant (K_{SV})(M^{-1}) of the respective GQDs in the presence of 4-acetamido-TEMPO free radicals recorded at different temperatures

T(°C)	GQDs	N-GQDs	SN-GQDs
25	1.05×10^4	9.56×10^4	1.2×10^5
32	9.8×10^3	8.3×10^4	1.03×10^5
40	8.9×10^3	6.1×10^4	9.2×10^4

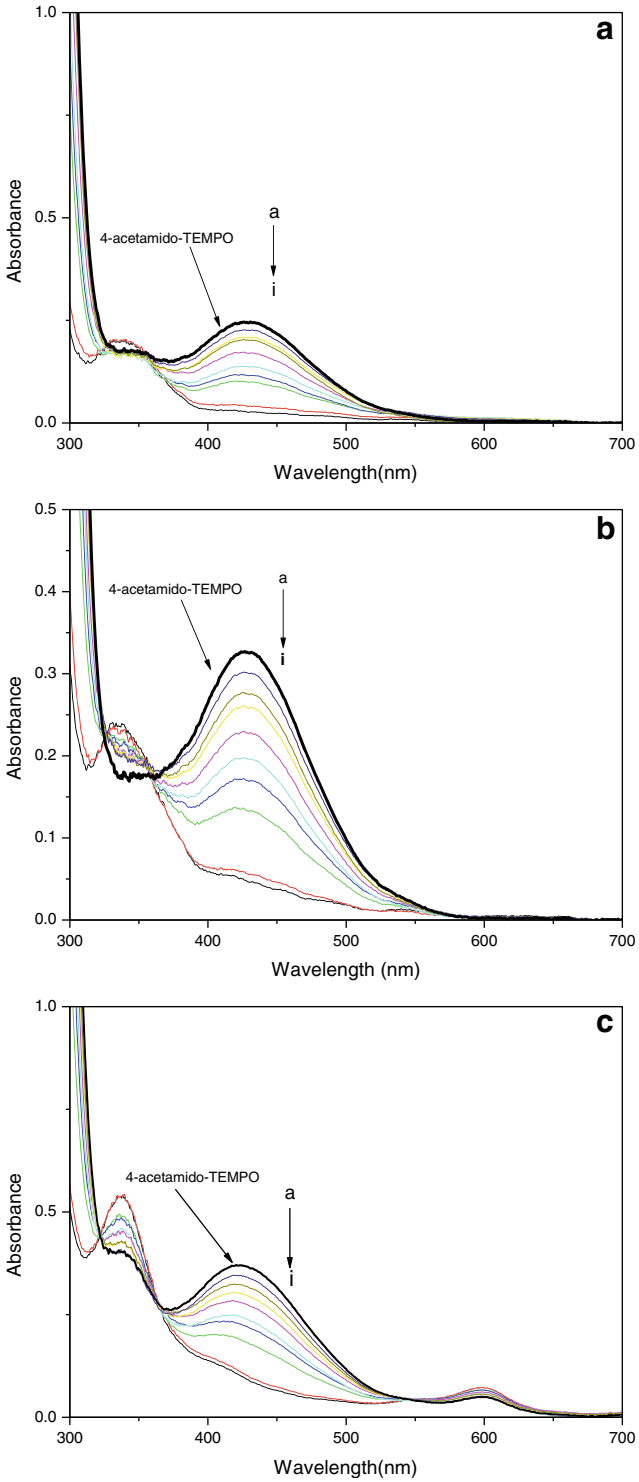

Fig. 11 UV-Vis absorption spectral changes (observed with time) following addition of **a** pristine GQDs, **b** N-GQDs and **c** SN-GQDs to 6 μM of 4-acetamido-TEMPO. (*a*) in the absence of GQDs, and b-i at 0.08, 0.17, 0.25, 0.5. 1, 4, 6, 10, 12, 15 h following addition of 1.0 mg/mL GQDs. Solvent: PBS buffer (pH 9.2) solution

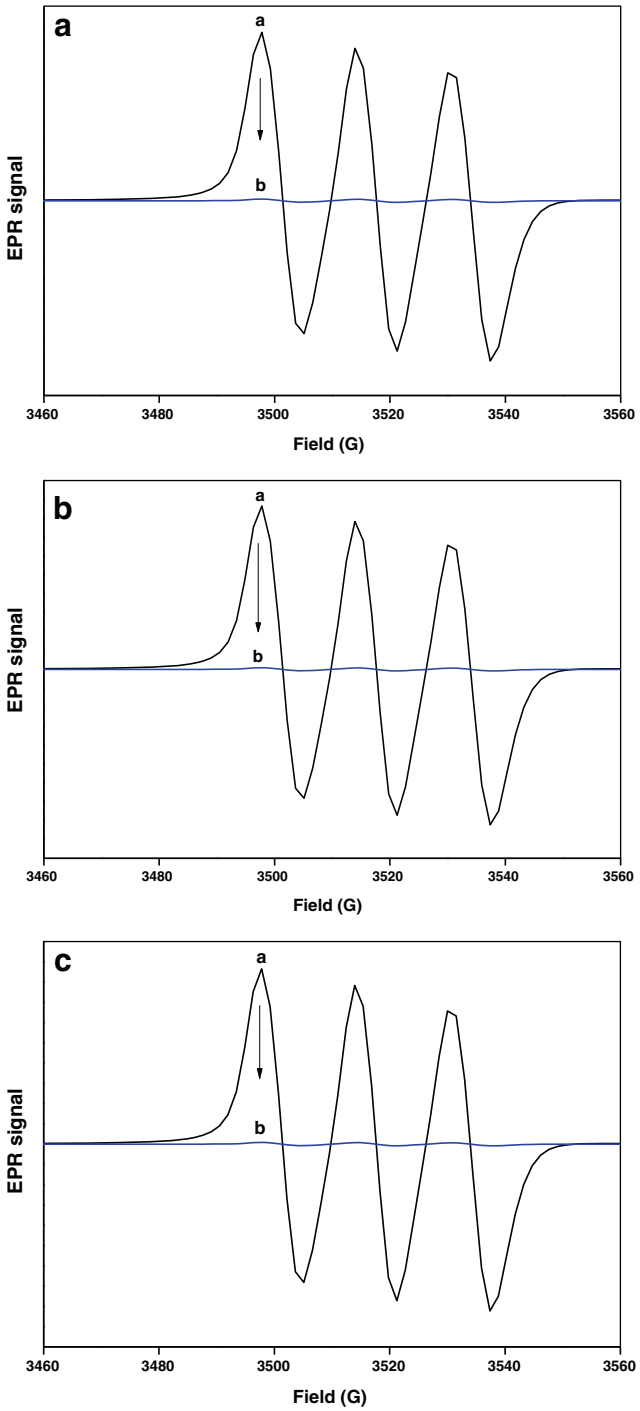

Fig. 12 EPR Spectra of 4-acetamido-TEMPO (20 mM) and upon addition of **a** GQDs, **b** N-GQDs and **c** SN-GQDs. [GQDs] = 400 μL of 1 mg/mL. Solvent: 50 mM PBS buffer pH 9.2. a and b denote 4-acetamido-TEMPO EPR signals before and after interaction with GQDs respectively

acetamido-TEMPO acted as the electron acceptor. This study holds promise for the fabrication of fluorescent nanoprobes as new sensing platform for antioxidants, organic radicals and importantly, intracellular fluorescence detection and imaging of biomolecules.

Acknowledgments This work was supported by the Department of Science and Technology (DST) and National Research Foundation (NRF), South Africa, through DST/NRF South African Research Chairs Initiative for Professor of Medicinal Chemistry and Nanotechnology (UID 62620) as well as Rhodes University/DST Centre for Nanotechnology Innovation, Rhodes University, South Africa.

Compliance with Ethical Standards

Conflicts of Interest There are no potential conflicts of interest with regard to this manuscript.

Funding The funders have agreed to publication.

Human and Animal Studies The research does not involve human participants and/or Animals.

References

1. Dong Y, Chen C, Zheng X, Gao L, Yu H, Quan X (2012) One-step and high yield simultaneous preparation of single and multi-layer graphene quantum dots from CX-72 carbon black. Journal of Materials Chemistry 22:8764–8766
2. Li L, Wu G, Hong T, Yin Z, Sun D, Abdel-Halim ES, Zhu JJ (2014) Graphene quantum dots as fluorescence probes for turn-off sensing of melanine in the presence of Hg^{2+}. ACS Appl Mater Interfaces 6: 2858–2864
3. Ge J, Minhuan L, Zhou B, Liu W, Guo L, Wang H, Jia Q, Niu G, Huang X, Zhou H, Xiangmin M, Pengfei W, Chun-Sing L, Zhang W, Han X (2014) A graphene quantum dot photodynamic therapy agent with high singlet oxygen generation. Nature Commun 5:4596
4. Zhu S, Zhang J, Liu X, Li B, Wang X, Tang S, Meng Q, Li Y, Shi C, Hu R, Yang B (2012) Graphene quantum dots with controllable surface oxidation, tunable fluorescence and up-conversion emission. RSC Adv 2:2717–2720
5. Li L, Wu G, Yang G, Peng J, Zhao J, Zhu JJ (2013) Focusing on luminescent graphene quantum dots: current status and future perspectives. Nanoscale 5:4015–4039
6. Zhu S, Song Y, Zhao X, Shao J, Zhang J, Yang B (2015) The photoluminescence mechanism in carbon dots (graphene quantum dots, carbon nanodots, and polymer dots): current state and future perspective. Nano Research 8:355–381
7. Tetsuka H, Asahi R, Nagoya A, Okamoto K, Tajima I, Ohta R, Okamoto A (2012) Optically tunable amino-functionalized graphene quantum dots. Adv Mater 24:5333–5338
8. Jin SH, Kim DH, Jun GH, Hong SH, Jeon S (2013) Tuning the photoluminescence of graphene quantum dots through the charge transfer effect of functional groups. *ACS Nano* 7:1239–1245
9. Wang Y, Zhang L, Liang RP, Bai JM, Qiu J (2013) Using Graphene Quantum Dots as Photoluminescent Probes for Protein Kinase Sensing, *Anal. Chem 85*:9148–9155
10. Li X, Zhu S, Xu B, Ma K, Zhang J, Yang B, Tian W (2013) Self-assembled graphene quantum dots induced by cytochrome c: a novel biosensor for trypsin with remarkable fluorescence enhancement. Nanoscale 5:7776–7779
11. Yuezhen H, Wang X, Sun J, Jiao S, Chen H, Gao F, Wang L (2014) Fluorescent blood glucose monitor by hemin-functionalized graphene quantum dots based sensing system. Analytica Chimica Acta 810:71–78
12. Huang H, Liao L, Xu X, Zou M, Liu F, Li N (2013) The electron-transfer based interaction between transition metal ions and

photoluminescent graphene quantum dots (GQDs): A platform for metal ion sensing. Talanta 15:152–157
13. Wu Z, Li W, Chen J, Yu C (2014) A graphene quantum dot-based method for the highly sensitive and selective fluorescence turn on detection of biothiols. Talanta 119:538–543
14. Fan L, Hu Y, Wang X, Zhang L, Li F, Han D, Li Z, Zhang Q, Wang Z, Niu L (2012) Fluorescence resonance energy transfer quenching at the surface of graphene quantum dots for ultrasensitive detection of TNT. Talanta 101:192–197
15. Adegoke O, Chidawanyika W, Nyokong T (2012) Interaction of CdTe quantum dots with 2,2-diphenyl-1-picrylhydrazyl free radical: a spectroscopic, fluorimetric and kinetic study. J Fluoresc 22: 771–778
16. Adegoke O, Hosten E, McCleland C, Nyokong T (2012) CdTe quantum dots functionalized with 4-amino-2,2,6,6-tetramethylpiperidine-N-oxide as luminescent nanoprobe for the sensitive recognition of bromide ion. Anal Chim Acta. 721:154–161
17. Tshangana C, Nyokong T (2015) The photophysical properties of multi-functional quantum dots-magnetic nanoparticles – indium octacarboxy phthalocyanine nanocomposite, J. Fluorescence 25: 199–210
18. Qu D, Zheng M, Zhang L, Zhao H, Xie Z, Jing X, Raid EH, Fan H, Sun Z (2014) Formation mechanism and optimization of highly luminescent N-doped graphene quantum dots. *Scientific Reports* 4:1–9
19. Qu D, Zheng M, Du P, Zhou Y, Zhang L, Li D, Tan H, Zhao Z, Xied Z, Sun Z (2013) Highly luminescent S, N co-doped graphene quantum dots with broad visible absorption bands for visible light photocatalysts. Nanoscale 5:12272–12277
20. Fery-Forgues S, Lavabre D (1999) Are fluorescence quantum yields so tricky to measure? A demonstration using familiar stationery products. J Chem Ed. 76:12660–11264
21. Fischer S, Georges J (1996) Fluorescence quantum yield of Rhodamine 6G in ethanol as a function of concentration using lens spectrometry. Chemical physics letters. 260:115–118
22. Yuan F, Ding L, Li Y, Li X, Fan L, Zhou S, Fang D, Yang S (2015) Multicolor fluorescent graphene quantum dots colorimetrically responsive to all-pH and a wide temperature range. Nanoscale. 7: 11727–11733
23. Benitez-Martinez S, Valcarcel M (2014) Graphene quantum dots as sensor for phenols in olive oil. Sensors and Actuators B 197:350–357
24. Tianju F, Wenjin Z, Wei T, Chunqiu Y, Songzhao T, Kaiyu C, Yidong L, Wei, H, Yong M, Arthur, E (2015) Controllable size-selective method to prepare graphene quantum dots from graphene oxide. Nanoscale Research Letters 10:1–8
25. Chua CK CK, Sofer Z, Šimek P, Jankovský O, K KÍ, Bakardjieva S, Kučková SH, Pumera M (2015) Synthesis of Strongly Fluorescent Graphene Quantum Dots by Cage-Opening Buckminsterfullerene. ACS Nano 9:2548–2555
26. Pan D, Zhang J, Li Z, Wu M (2010) Hydrothermal route for cutting graphene sheets into blue-luminescent graphene quantum dots. Adv Mater 22:734–738
27. Dong Y, Lin J, Chen Y, Fu F, Chi Y, Chen G (2014) Graphene quantum dots and graphite nanocrystals in coal. Nanoscale 6: 7410–7415
28. Zheng XT, Ananthanarayanan KQ, Luo P, Chen P (2015) Glowing Graphene Quantum Dots and Carbon Dots: Properties, Syntheses, and Biological Applications. Small 11:1620–1636
29. Feng Y, Zhao J, Yan X, Tang F, Xue Q (2014) Enhancement in the fluorescence of graphene quantum dots by hydrazine reduction. Carbon 66:334–339
30. Hu Y, Zhao G, Lu N, Chen Z, Zhang H, Li H, Shao L, Qu L (2013) Graphene quantum dots-carbon nanotubes hybrid arrays for supercapacitors. *Nanotechnology*. doi:10.1088/0957-4484/24/19/195401
31. Chien C, Li S, Lai W, Yeh Y, Chen H, Chen I, Chen L, Nemoto IS (2012) Tunable photoluminescence from graphene oxide. Angew Chem Int Ed 51:6662–6666
32. Wei D, Wei Z, Chen S, Qi X, Yang T, Hu J, Wang D, Li-Jun W, Shahnaz F, Li L (2013) Space-confinement-induced synthesis of Pyridinic- and pyrollic-Nitrogen doped graphene for the catalysis of oxygen reduction. Angew Chem Int Ed 52:11755–11759
33. Sen VD, Golubev VA (2009) Kinetics and mechanism for acid catalyzed disproportionation of 2,2,6,6 tetramethylpiperidine-1-oxyl. J Phys Org Chem 22:138–143
34. Sun H, Wu L, Wei W, Qu X (2013) Recent advances in graphene quantum dots for sensing. Mater Today 11:433–442
35. Fengxiang W, Zhenyan G, Wu L, Wenjan W, Xifeng X, Qingli H (2014) Graphene quantum dots as fluorescent sensing platform for highly efficient detection of copper (II) ions. Sensors and Actuators B 190:516–522
36. Chakraborti H, Sinha S, Ghosh S, Pal SK (2013) Interfacing water soluble nanomaterials with fluorescence chemosensing: graphene quantum dots to detect Hg^{2+} in 100 % aqueous solution. Materials letters 97:78–80
37. Murov SL, Carmichael I (1993) Hug GL in: "Handbook of Photochemistry" 2nd edition, Decker M. New York 207
38. Liu EH, Qi LW, Li P (2010) Structural Relationship and Binding Mechanisms of Five Flavonoids with Bovine Serum Albumin. Molecules 15:9092–9103